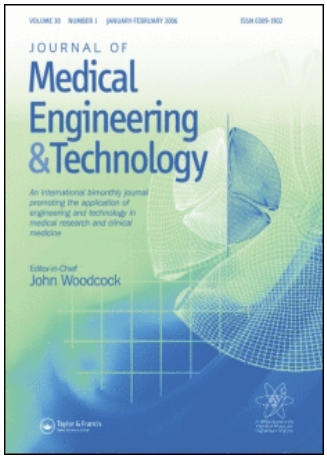

Journal of Medical Engineering & Technology
Publication details, including instructions for authors and subscription information:
http://www.informaworld.com/smpp/title~content=t713736867

Extraction and reconstruction of retinal vasculature

M. H. Ahmad Fadzil [a]; Lila Iznita Izhar [a]; P. A. Venkatachalam [a]; T. V. N. Karunakar [b]
[a] Intelligent Imaging Technology Group, Electrical and Electronic Engineering Programme, Universiti Teknologi PETRONAS, Tronoh, Perak, Malaysia
[b] Ophthalmology Department, General Hospital, Kuala Lumpur, Malaysia

Online Publication Date: 01 November 2007
To cite this Article: Fadzil, M. H. Ahmad, Izhar, Lila Iznita, Venkatachalam, P. A. and Karunakar, T. V. N. (2007) 'Extraction and reconstruction of retinal vasculature', Journal of Medical Engineering & Technology, 31:6, 435 - 442
To link to this article: DOI: 10.1080/03091900601111201
URL: http://dx.doi.org/10.1080/03091900601111201

Journal of Medical Engineering & Technology, Vol. 31, No. 6, November/December 2007, 435–442

Extraction and reconstruction of retinal vasculature

M. H. AHMAD FADZIL†, LILA IZNITA IZHAR†, P. A. VENKATACHALAM† and T. V. N. KARUNAKAR‡

†Intelligent Imaging Technology Group, Electrical and Electronic Engineering Programme, Universiti Teknologi PETRONAS, Bandar Sri Iskandar, 31750 Tronoh, Perak, Malaysia.
‡Ophthalmology Department, General Hospital, Kuala Lumpur, Malaysia.

Information about retinal vasculature morphology is used in grading the severity and progression of diabetic retinopathy. An image analysis system can help ophthalmologists make accurate and efficient diagnoses. This paper presents the development of an image processing algorithm for detecting and reconstructing retinal vasculature. The detection of the vascular structure is achieved by image enhancement using contrast limited adaptive histogram equalization followed by the extraction of the vessels using bottom-hat morphological transformation. For reconstruction of the complete retinal vasculature, a region growing technique based on first-order Gaussian derivative is developed. The technique incorporates both gradient magnitude change and average intensity as the homogeneity criteria that enable the process to adapt to intensity changes and intensity spread over the vasculature region. The reconstruction technique reduces the required number of seeds to near optimal for the region growing process. It also overcomes poor performance of current seed-based methods, especially with low and inconsistent contrast images as normally seen in vasculature regions of fundus images. Simulations of the algorithm on 20 test images from the DRIVE database show that it outperforms many other published methods and achieved an accuracy range (ability to detect both vessel and non-vessel pixels) of 0.91–0.95, a sensitivity range (ability to detect vessel pixels) of 0.91–0.95 and a specificity range (ability to detect non-vessel pixels) of 0.88–0.94.

Keywords: Retinal vasculature detection and reconstruction; Region growing; Gaussian derivative

1. Introduction

Diabetic retinopathy (DR), a long term complication of diabetes due to the damage on the retinal vasculature, is the leading cause of blindness in the world. In Malaysia, the diabetic population has increased over four-fold from 300 000 in 1996 [1] to nearly 1.4 million in 2005 [2]. About 30% of the diagnosed diabetic population in 1996 has retinopathy and each year 1% develops sight-threatening retinopathy [1]. The major problem in the early detection and treatment of DR is the large number of patients, which can hamper effective screening using direct ophthalmoscopy.

Analysing and interpreting fundus images have become necessary and important diagnostic procedures in ophthalmology. Among the features in ocular fundus images, the structure of the retinal vessel plays an important role in revealing the severity of DR and other eye related diseases, besides being taken as landmarks for image-guided laser treatment of choroidal neovascularization and for localization of optic nerve, fovea and lesions [3–5]. As well as enabling the detection of abnormal growth of new vessels, detection of retinal vasculature can also assist in the analysis of the capillary free zone and the foveal avascular zone (FAZ) [6,7].

Reliable methods are needed to extract vascular structures for analysis. Generally, there are four main approaches that have been identified: the edge detection approach [8,9], the matched filter approach [5,10,11],

*Corresponding author. Email: fadzmo@petronas.com.my

Journal of Medical Engineering & Technology
ISSN 0309-1902 print/ISSN 1464-522X online © 2007 Informa UK Ltd.
http://www.tandf.co.uk/journals
DOI: 10.1080/03091900601111201

the tracking-based approach [5,10,12] and the mathematical morphology transformation approach [3,4,13,14]. The edge detection approach suffers from poor performance in low contrast fundus images. It is reported in [3,10,11] that, to overcome this problem, an inverted Gaussian-shaped zero-sum matched filter is used. Even though primary (large) vessels are successfully detected, this approach tends to give false detection at the boundary of bright regions. The tracking-based approach is an extension of the edge detection whereby the edge map provides location of the vessel borders. Missing edges especially at bifurcations create discontinuity in vessel tracking that require edge-line regeneration methods. An algorithm that combines morphological filters and curvature evaluation to segment vessels has been developed [4]. A combination of top-hat transformations and Laplacian transforms was used to highlight vessels. This approach generates a more detailed description of the vascular structure. However, it tends to miss important bifurcation and intersection points. To overcome this problem, a dynamic local region growing is used to recover and reconstruct missing and partially detected vessels [3].

The objective of this research is to develop a computer vision based diagnostic tool that enables ophthalmologists to screen and grade DR. In this paper, the development of an algorithm to detect and reconstruct complete retinal vasculature in low and inconsistent contrast colour fundus images (no contrast agent used) is discussed.

2. Analysis of retinal vasculature

In this work, enhancement, extraction and reconstruction of retinal vasculature using image analysis techniques are being developed. A flowchart for the image analysis is shown in figure 1. The process is divided into two blocks, vessel extraction and vessel reconstruction. Figure 2 shows three types of reference images used, namely reference model image A, reference model image B and reference colour fundus image.

Reference model image A is designed to measure the performance of the vessel extraction algorithm for various sizes of vessels at varying levels of contrast. It is also designed to measure the performance of region growing in vessel reconstruction. There are 11 vertical lines with different widths ranging from 2 to 12 pixels. Each line has seven different intensity regions; the darkest (grey-level value = 52) at the bottom to the lightest (grey-level value = 64) at the top. Thus, the contrast level for each region in each line ranges from 4 to 16 in intensity between the lines and background. The background is uniform at a higher intensity level (grey-level value = 68) relative to the lines. Reference model image B represents the fundus image with artificial optic disk and FAZ and curving lines representing vessels with width ranging from 2 to 12 pixels (7–42 μm). The background is not uniform but is maintained at a higher intensity level relative to the vessels. The fundus image used is a typical colour image of the retina of DR patients. In the development of the algorithm, reference model images A and B are used initially before applying the reference fundus image. In this way, the performance of the algorithm can be determined and any problems can be detected.

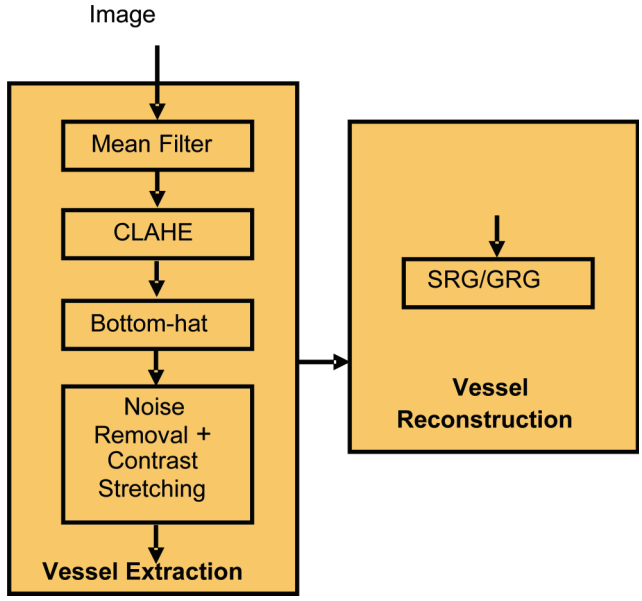

Figure 1. A flowchart of the algorithm.

2.1. Vessel extraction

The green band image is used, as the vessels are relatively darker compared to the normal intensity image. For pre-processing, a 3×3 mean filter is applied to the green image to reduce the noise effects and false segmentation on the boundary of camera's aperture [15]. Contrast limited adaptive histogram equalization (CLAHE) [16] is then applied to enhance vessels. CLAHE partitions the image into contextual regions and applies the histogram equalization to each one. This process evens out the distribution of used grey-level values and thus makes hidden features of the image more visible. By applying CLAHE to the reference model image B, it can be seen that in figures 3 and 4 vessels in both bright and dark regions are contrast-enhanced equally well, whilst the typical contrast stretching is not.

In this work, the extraction of dark objects (vessels) on background of higher intensity level is achieved by using a morphological filter called bottom-hat, expressed as follows:

$$\text{Dark objects(vessels)} : \text{Bottom-hat}(I, B) = (I \bullet B) - I \quad (1)$$

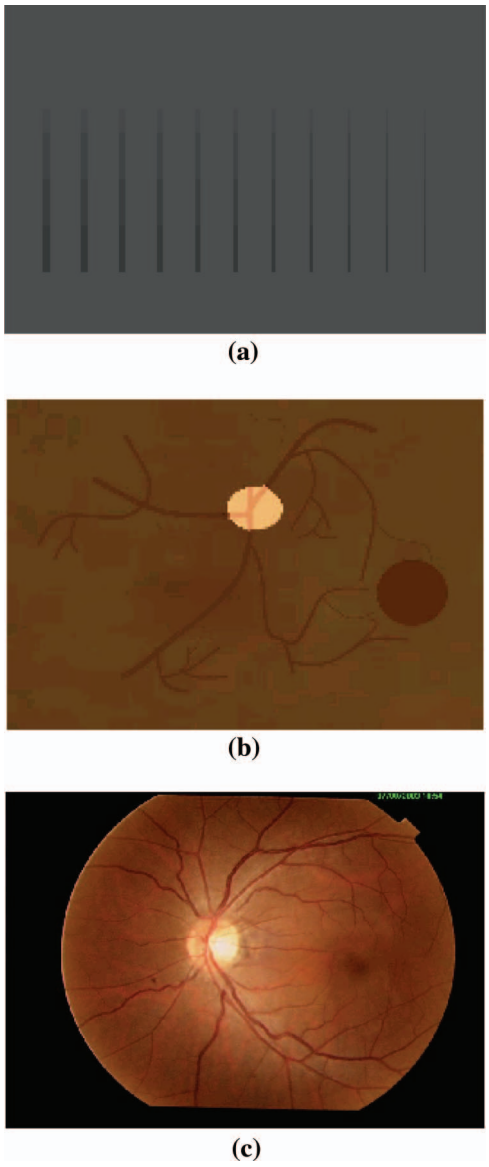

Figure 2. (a) Reference model image A; (b) reference model image B; (c) reference fundus image.

In bottom-hat, morphological closing (•) of the input image, $I(x,y)$ by a structuring element, $B(x,y)$ is performed followed by subtraction of the resultant image by the input image. Note that the closing operation is defined as the dilation of an object followed by the erosion of the dilated object using the same structuring element.

The structuring element (SE) used is of linear type [3,4]. The size of the element is critical because portions of vessels with profiles larger than the SE will be excluded. However, using larger SE can cause more objects representing non-vessels to be extracted. The primary vessels are 10–12 pixels wide. The branching and intersection points of vessels are wider by 2–3 pixels than the vessels. To ensure that the primary vessels (that are normally 10–12 pixel wide) including their branching and intersection points can be extracted, an SE size of 15 is used. In this process, the SE is posed in different orientations using a rotating angle (at incremental of 15°) from 0 to 180°. A sum of bottom-hats using 12 linear SEs allows all vessels to be extracted in low local contrast regions regardless of their sizes and directions, as shown:

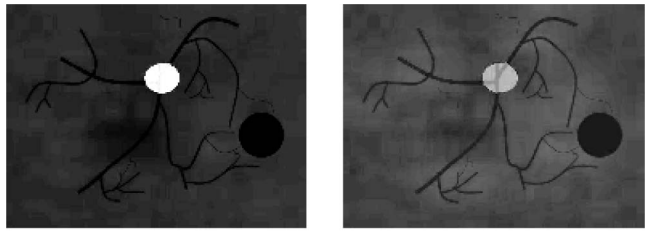

Figure 3. Reference model image B after (a) contrast stretching; (b) CLAHE.

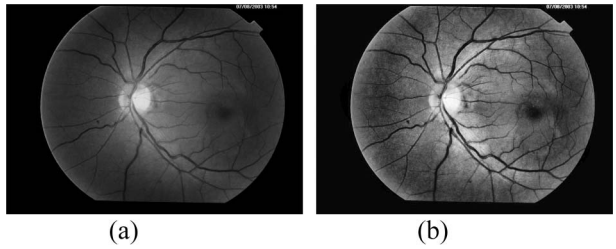

Figure 4. Reference fundus image after (a) contrast stretching; (b) CLAHE.

$$\text{Sum of Bottom-hat}(I, B_{12}) = \sum_{i=1}^{12}((I \bullet B_i) - I) \qquad (2)$$

To eliminate image artefacts in the enhanced background (refer to figure 5), a noise removal process is carried out. Here, we obtain the background image, BG by applying averaging filter of size 40×40 pixels on the sum of bottom-hat image. In the removal process, the sum of bottom-hat image is subtracted by the background image, BG. Contrast stretching is applied after background noise removal to improve the contrast of extracted vessels. Here, a linear scaling function is applied to the image pixel values so that the range of intensity values of the image is spanned over a desired range of values. Figure 5 shows the images after applying bottom-hat and subsequent application of background noise removal with contrast stretching on the reference images.

2.2. *Vessel reconstruction*

Morphological transformations may miss out some important bifurcations and intersection points, which are required for a complete morphology of vascular structure.

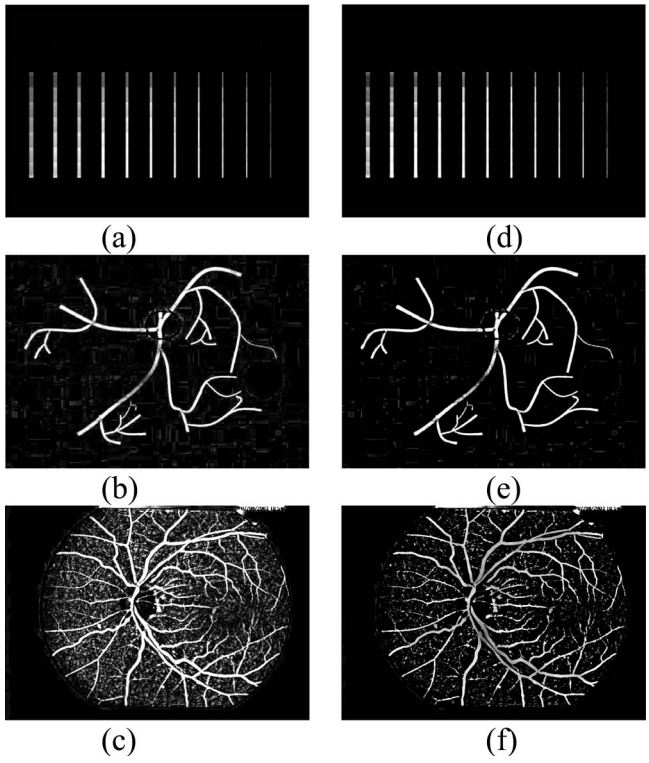

Figure 5. Vessel extraction of reference images (a–c) after applying sum of bottom-hat, and (d–f) after subsequent application of background noise removal.

Furthermore, there are still some remaining background noise and artefacts at the background. To overcome this, a morphology reconstruction process is performed based on region growing. Region growing has been known to perform well on segmenting foreground from a noisy background image. At an earlier stage of this work, seed-based region growing (SRG) [17,18] was applied to reconstruct the retinal vasculature. Figure 6 compares the application of SRG with one seed pixel placed on each vessel line and five seed pixels placed on each vessel line for reference model image A.

Figure 7 compares the application of SRG with five seeds and 16 seeds for reference model image B. Figure 8 compares the application of SRG with seven seed pixels and 18 seed pixels for the reference fundus image. SRG performs better with more initial seed pixels.

However, in applications such as fundus images, the initial placement of seed pixels can be time consuming (due to selecting appropriate number of seed pixels and their locations) and can lead to inconsistent results. It is also reported that SRG can cause over segmentation at vessel boundaries (also referred to as the partial volume effect) [19,20].

A gradient-based region growing (GRG) method has been developed to overcome the above problems associated with SRG and to improve the accuracy of vessel

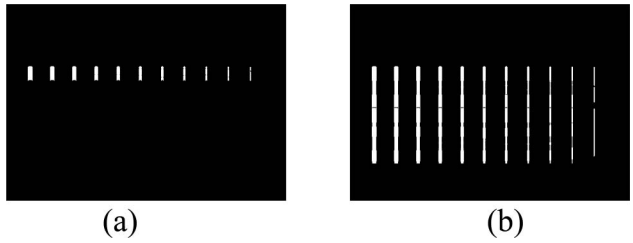

Figure 6. SRG resultant images of reference model image A: (a) one seed pixel for each vessel line; (b) five seed pixels for each vessel line.

Figure 7. SRG resultant images of reference model image B: (a) five seed pixels; (b) 16 seed pixels.

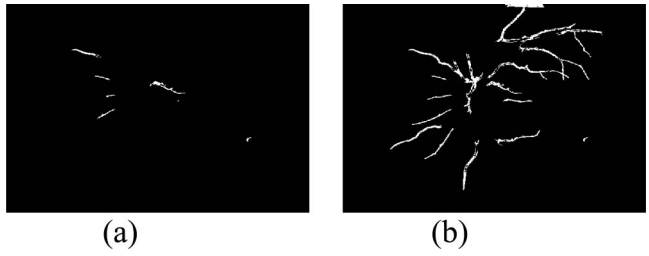

Figure 8. Vessel reconstruction using SRG on the reference fundus image: (a) seven seed pixels; (b) 18 seed pixels.

reconstruction. In GRG two homogeneity criteria are used, namely change of gradient magnitude and average intensity change. The gradient magnitude change is used to identify ambiguous boundaries between homogeneous regions and to resolve the partial volume effect problem on the boundary [19]. In GRG, the image with extracted vessels $I(x, y)$ is convolved with a first order Gaussian derivative kernel to give the gradient image, $I_{\Delta}(x, y)$ followed by region growing. The gradient image or first-order Gaussian derivative is estimated as follows:

$$I_{\Delta}(x,y) = I(x,y) * \frac{\partial G(x,y,\sigma)}{\partial x \partial y}, \tag{3}$$

$$G(x,y,\sigma) = \frac{1}{2\pi\sigma^2} \exp^{\frac{-(x^2+y^2)}{2\sigma^2}} \tag{4}$$

By using the Gaussian derivative kernel, sensitivity to noise in the gradient image is reduced. The kernel size is set to 15×15 pixels and σ is set to 0.5 to ensure accurate identification of vessel border. From analysis on gradient images, the ranges of gradient magnitude change, $GMAG_{\min}$ at the vessel border, are obtained; 70–228 for reference model image A and 86–230 for reference model image B and fundus images.

A 3×3 window is centred at the seed pixel, $S_{x,y}$, and the average intensity value $A_{x,y}$ in the window is computed to obtain image, $I_{avg}(x,y)$, as the other homogeneity criterion. If the difference in intensity between the seed pixel and the average value is smaller than a threshold at a particular point, i.e.:

$$|S_{x,y} - I_{avg}(x,y)| \leq T\_\text{int}_{x,y} \tag{5}$$

and if at seed-pixel location $S_{x,y}$ the gradient magnitude change is smaller than $GMAG_{\min}$, i.e.:

$$\text{at } S_{x,y}: \quad I_{\Delta}(x,y) < GMAG_{\min} \tag{6}$$

the seed pixel is labelled homogeneous to vessel pixels and the process is repeated for the next seed pixel location, or else the seed pixel is labelled as a background pixel and the process stops. The $GMAG_{\min}$ is set to 100 for reference model A and 150 for reference model B and fundus images. The threshold $T\_\text{int}_{x,y}$ is defined as follows:

$$T\_\text{int}_{x,y} = \alpha I_{avg}(x,y), \alpha = 0.5 \sim 0.7 \tag{7}$$

Figure 9 depicts the gradient images of reference images A and B and the reference fundus image. In GRG, the selected homogeneity criteria that combine the intensity value with the gradient magnitude change enable the region growing process to adapt to intensity changes of the vessels. Therefore fewer seed pixels (fewer than 10 seed pixels) are required for GRG to perform vessel reconstruction, unlike SRG, which requires more than twice the amount of seed pixels required by GRG.

Figure 10(a) shows the resultant image of GRG with a seed pixel for each of the vessel lines in image A. Each vessel is successfully grown from an initial seed pixel placed in the region with intensity level of 73 to the region with intensity level of 255. Thus, the region growing process is able to adapt to intensity changes within vessel regions.

Similar results are obtained for reference model image B and the reference fundus image, as shown in figures 10(b) and (c). For reference model image B, five seed pixels are placed (figure 7(a)). For the reference fundus image, the seed pixels are chosen among vessel pixels located near the vessel ends (figure 8(a)). Here it can be seen that the GRG technique outperforms SRG in reconstructing the complete vessel network (compare figure 10(b) with figure 7 and figure 10(c) with figure 8).

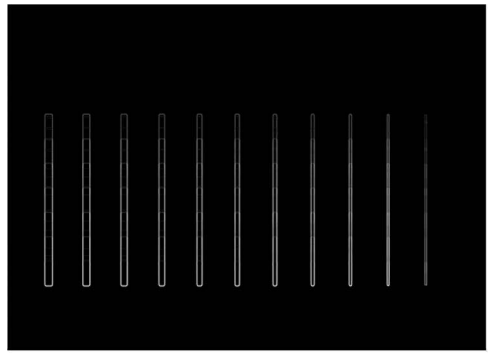

(a)

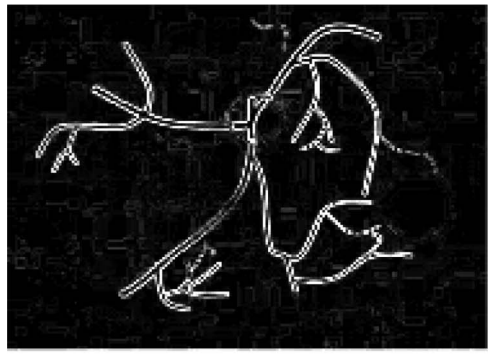

(b)

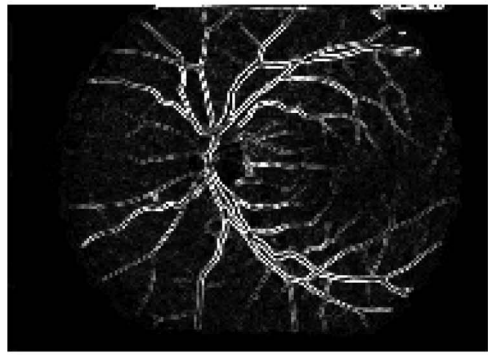

(c)

Figure 9. Gradient images by first-order gradient derivative for reference model: (a) image A; (b) image B; (c) fundus image.

3. Performance analysis

For performance analysis, the developed algorithm is tested and evaluated on 20 non-mydriatic images from the DRIVE database [21,22]. The images are captured in digital form from a Canon CR5 non-mydriatic 3CCD camera at 45° field of view (FOV). The images are of size 584×565 pixels, 8 bits per colour channel. The FOV of each image is circular with a diameter of approximately 540 pixels. These images have been hand-labelled (manually segmented) by three observers trained by an ophthalmologist. The images used in this work are

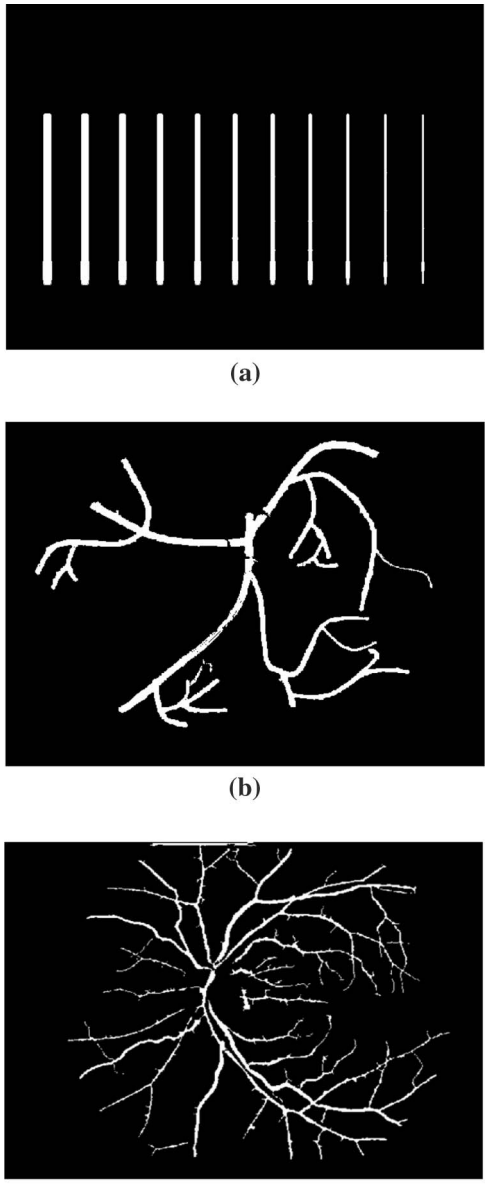

Figure 10. Vessel reconstruction of reference images using GRG: (a) image A with five seed pixels; (b) image B with five seed pixels; (c) fundus image with seven seed pixels.

manually segmented twice, resulting in sets A and B. In set A, 12.7% of pixels were marked as vessel, against 12.3% for set B. In the analysis, reconstructed retinal vasculatures of the 20 test images are compared against the segmentations of set A.

In the performance analysis, the detected vessels classified as vessels are considered as true positives (TP) and the detected vessels classified as non-vessels are considered as false positives (FP). For true negatives (TN), detected non-vessels that are classified as non-vessels will be considered whereas for false negatives (FN), detected non-vesssels that are classified as vessels will be considered [23].

Let $C(x,y)$ be the automatically reconstructed (segmented) image by the algorithm, and $G(x,y)$ be the manually segmented image of set A from the DRIVE database. The fraction of true positive (TP) and false positive (FP) and true negative (TN) and false negative (FN) negative are determined as follows [23]:

$$\text{TN fraction}: \quad \frac{\sum_{all\,x,y}[C(x,y)=G(x,y)=0]}{\sum_{all\,x,y}[(C(x,y)=0)]}. \tag{8}$$

$$\text{TP fraction}: \quad \frac{\sum_{all\,x,y}[C(x,y)=G(x,y)=1]}{\sum_{all\,x,y}[(C(x,y)=1)]}. \tag{9}$$

$$\text{FP fraction}: \quad \frac{\sum_{all\,x,y}[(C(x,y)=1)\wedge(G(x,y)=0)]}{\sum_{all\,x,y}[(C(x,y)=1)]} \tag{10}$$

$$\text{FN fraction}: \quad \frac{\sum_{all\,x,y}[(C(x,y)=0)\wedge(G(x,y)=1)]}{\sum_{all\,x,y}[(C(x,y)=0)]} \tag{11}$$

From the above values, it is easy to compute the accuracy (ability to detect vessels and non-vessels) of the algorithm. There are two other parameters that are used to measure performance of the algorithm, namely the ability to detect vessels (sensitivity) and the ability to detect non-vessels (specificity) [5,24].

Accuracy, specificity and sensitivity are computed as shown below:

$$\text{Accuracy} = \text{TP} + \text{TN}/\text{FOV} \tag{12}$$

$$\text{Specificity} = \text{TN}/(\text{TN} + \text{FP}) \tag{13}$$

$$\text{Sensitivity} = \text{TP}/(\text{TP} + \text{FN}) \tag{14}$$

Ideally, the performance of a segmentation algorithm should results in small FP and FN fractions (FP, FN 0) and large TP and TN fractions (TP, TN $\rightarrow$ 1). Following from this, the accuracy, specificity and sensitivity performance parameters should trend toward a value of 1.

Based on the simulation of detecting and reconstructing retinal vasculature in 20 test images from the DRIVE database, the fractions of TP, FP, TN, FN, and the performance parameters (accuracy, specificity and sensitivity) are shown in table 1. It can be seen from this table that the algorithm can detect and reconstruct vessel (sensitivity) between 91–95% and non-vessels (specificity) between 88–94%. Over-segmentation (FP) is kept low at 6–16% whilst under-segmentation (FN) is at 4–9%. The overall accuracy of the algorithm is between 91% and 95%. The standard deviations obtained for each range are small.

Table 1. Performance parameters obtained based on 20 test images of the DRIVE database.

Performance parameters	Range	Mean	Std
True positive (TP)	0.86–0.94	0.9070	0.0255
False positive (FP)	0.06–0.16	0.0900	0.0253
True negative (TN)	0.90–0.96	0.9400	0.0128
False negative (FN)	0.04–0.09	0.0600	0.0128
Accuracy	0.91–0.95	0.9316	0.0216
Sensitivity	0.91–0.95	0.9335	0.0111
Specificity	0.88–0.94	0.9084	0.0110

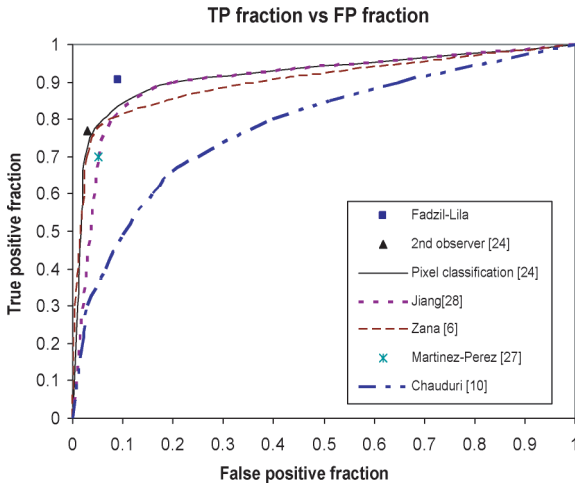

Figure 11. Graph showing TP fraction vs. FP fraction.

Table 2. Accuracy achieved by the published methods reproduced from Niemeijer [21].

Method	Accuracy
2nd observer [23]	0.9474
Pixel classification [23]	0.9416
Zana and Klein [4]	0.9377
Fadzil-Lila	0.9316
Jiang and Mojon [25]	0.9212
Perez *et al.* [26]	0.9181
Chaudhuri *et al.* [11]	0.8773

Figure 11 is a plot of TP fraction against FP fraction depicting our test results (Fadzil-Lila) and results of other researchers, i.e. hand-labelled by 2nd observer [21], pixel classification [21], Jiang and Mojon [25], Zana and Klein [4], Perez *et al.* [26] and Chauduri *et al.* [11] using images from the DRIVE database for comparison. Given that it is required for TP to be close to 1 and FP to be close to 0, it can be seen in figure 11 that the proposed algorithm (Fadzil-Lila) outperforms other methods.

Table 2 compares the developed algorithm with other published methods based on the accuracy performance parameter. If based on the accuracy parameter, the method is found to be comparable to other methods such as pixel classification [23] and by Zana and Klein [4].

4. Conclusion

In this paper, image processing techniques are applied to extract and reconstruct the morphology of the complete vascular structure of the retina.

The fundus image is firstly enhanced using a mean filter followed by CLAHE and bottom-hat morphological transformation to extract retinal vasculature (blood vessels). It is found that CLAHE improves contrast by a factor of more than two for objects which are located in both bright and dark regions. A sum of bottom-hat with 12 linear structuring elements of size 15 and at 0–180° (incremental at 15°) is performed to ensure all blood vessels are extracted. Background noise removal is then carried out to reduce unwanted linear features at the background being enhanced during bottom-hat. Further enhancement of vessels is then carried out using contrast stretching.

In vessel reconstruction, a region growing technique based on first-order Gaussian derivative (GRG) is performed on the extracted retinal vasculature. GRG incorporates both gradient magnitude change and average intensity as the homogeneity criteria that enable the process to adapt to intensity changes and intensity spread over the vasculature region. GRG thus reduces the required number of seeds to near optimal for the region growing process in reconstructing retinal vasculature. This overcomes the poor performance of current seed-based methods especially for low and inconsistent contrast images such as the vasculature region in fundus images. The gradient magnitude change in GRG is also used to identify ambiguous boundaries between homogeneous regions and resolve the partial volume effect (over segmentation) problem on the boundary.

Performance analysis indicates that the accuracy, specificity and sensitivity of the algorithm on vessel detection and reconstruction achieved ranges of 91–95%, 88–94% and 91–95%, respectively. The algorithm is both reliable and effective in detecting and reconstructing the vascular structure of colour fundus images, given that the range of the true positive fraction is high and the range of the false positive fraction is low.

References

[1] National Malaysian Eye Survey, 1996, Screening for Diabetic Retinopathy. Ministry of Health, Malaysia.

[2] Disease Center: Wrong Diagnosis, Statistics by Country for Type 2 Diabetes. Available online at: http://www.wrongdiagnosis.com/d/diab2/stats-country.htm (accessed November 2004).

[3] Fang, B., Hsu, W. and Lee, M.L., 2003, Reconstruction of vascular structures in retinal images. *IEEE International Conference on Image Processing*, Barcelona, 14–17 September 2003, vol. II, pp. 157–160.

[4] Zana, F. and Klein, J.C., 2001, Segmentation of vessel-like patterns using morphology and curvature evaluation. *IEEE Transactions on Image Processing*, **10** (7), 1010–1019.

[5] Hoover, A., Kouznetsova, V. and Goldbaum, M., 2000, Locating blood vessels in retinal images by piecewise threshold probing of a matched filter response. *IEEE Transactions on Medical Imaging*, **19** (3), 337–346.

[6] Ballerini, L., 1998, Detection and quantification of foveal avascular zone alterations in diabetic retinopathy. *Internet World Congress for Biomedical Sciences – INABIS*. On-line Proceedings of the 5th Internet World Congress for Biomedical Sciences 1998 (INABIS) at McMaster University, Canada, 7th–16th December. (Available online at: http://www.mcmaster.ca/inabis98/ophthalmology/ballerini0155/two.html)

[7] Ibanez, M.V. and Simo, A., 1999, Bayesian detection of the fovea in eye fundus angiographies. *Pattern Recognition Letters*, **20,** 229–240.

[8] Li, H. and Chutatape, O., 2000, Fundus image features extraction, *Proceedings of the 22nd Annual EMBS International Conference*, Chicago, IL, 23–28 July, pp. 3071–3073.

[9] Elena, M., Perez, M., Hughes, A.D., Stanton, A.V., Thom, S.A., Bharath, A.A. and Parker, K.H., 1999, Segmentation of retinal blood vessels based on the second directional derivative and region growing. *IEEE International Conference on Image Processing*, **2,** 173–176.

[10] Zhou, L., Rzeszotarski, M.S., Singerman, L.J. and Chokreff, J.M., 1994, The detection and quantification of retinopathy using digital angiogram. *IEEE Transactions on Medical Imaging*, **13** (4), 619–626.

[11] Chaudhuri, S., Shatterjee, S., Katz, N., Nelson, M. and Goldbaum, M., 1989, Detection of blood vessels in retinal images using two- dimensional matched filters. *IEEE Transactions on Medical Imaging*, **8** (3), 263–269.

[12] Tamura, S., Okamoto, Y. and Yanashima, K., 1998, Zero-crossing interval correction in tracing eye fundus blood vessels. *Pattern Recognition*, **21,** 227–233.

[13] Gregson, P.H., Shien, Z., Scott, R.C. and Kozousek, V., 1995, Automated grading of venous beading. *Computer and Biomedical Research*, **28,** 291–304.

[14] Zana, F. and Klein, J.C., 1997, Robust segmentation of vessels from retinal angiography. *IEEE 13th International Conference on Digital Signal Processing*, 2–4 July, Santorini, Hellas, Greece, pp. 1087–1091.

[15] Conforth, D.J., Jelinek, H.J., Leandro, J.J.G., Soares, J.V.B., Cesar Jr, R.M., Cree, M.J., Mitchell, P. and Bossomaier, T., 2004, Development of retinal blood vessel segmentation methodology using wavelet transforms for assessment of diabetic retinopathy. *Eighth Asia Pacific Symposium on Intelligent and Evolutionary Systems*, 6–7 December 2004, Cairns, Australia, pp. 50–60.

[16] Jin, Y., Fayad, L. and Laine, A., 2001, Contrast enhancement by multi-scale adaptive histogram equalization. *Proceedings of SPIE*, **4478,** 206–213.

[17] Ngah, U.K., Hai, O.T. and Khalid, N.E.A., 2000, Mammographic calcification clusters using region growing technique. *Proceedings of the New Millenium International Conference on Pattern Recognition & Robot Vision [TATI]*, 14–15 May 2000, Terengganu, Malaysia.

[18] Venkatachalam, P.A., Fadzil, M.H. and Devan, K.S., 2005, Computer-aided detection and diagnosis of microcalcifications in digital mammography. An IRPA Grant Project of University Technology PETRONAS.

[19] Lee, Y.B., Song, S.M., Lee, J.S. and Kim, M.H., 2005, Tumor segmentation from small animal PET using region growing based on gradient magnitude. *IEEE International Conference on Communication*, 16–20 May 2005, Seoul, Korea.

[20] Sato, M., Lakare, S., Wan, M., Kaufman, A. and Nakajima, M., 2000, A gradient magnitude based region growing algorithm for accurate segmentation. *IEEE International Conference on Image Processing*, **3,** 448–451.

[21] Niemeijer, M., Staal, J., Ginnekan, B.V., Loog, M. and Abramoff, M.D., 2004, Comparative study of retinal vessel segmentation methods on a new publicly available database. In: J.M. Fitzpatrick and M. Sonka (Eds) *SPIE Medical Imaging*, **5370**, 648–656. Available online at: http://www.isi.uu.nl/Research/Databases (accessed January 2006).

[22] Staal, J.J., Abramoff, M.D., Neimeijer, M., Viergeer, M.A. and Ginneken, B.V., 2004, Ridge based vessel segmentation in color images of the retina. *IEEE Transactions on Medical Imaging*, **23,** 501–509.

[23] Fritzsche, K.H., 2002, Computer vision algorithms for retinal vessel width change detection and quantification. A proposal to conduct doctoral study. Available online at: http://www.cs.rpi.edu/~fritzk2/ken_candidacy.pdf (accessed February 2006).

[24] Walter, T., Klein, J.C., Massin, P. and Erginay, A., 2002, A contribution of image processing to the diagnosis of diabetic retinopathy—detection of exudates in color fundus images of the human retina. *IEEE Transactions on Medical Imaging*, **21,** 1236–1244.

[25] Jiang, X. and Mojon, D., 2003, Adaptive local thresholding by verification-based multithreshold probing with application to vessel detection in retinal images. *IEEE Transactions on Pattern Analysis and Machine Intelligence*, **25,** 131–137.

[26] Perez, M.M., Hughes, A.D., Stanton, A.V., Thom, S.A., Bharath, A.A. and Parker, K.H., 1999, Retinal Blood Vessel Segmentation by Means of Scale-Space Analysis and Region Growing, *Lecture Notes in Computer Sciences (MICCAI 99)*, Cambridge, England, 19–22 September, **1679,** 90–97.